Taylor & Francis
Taylor & Francis Group

Computer Methods in Biomechanics and Biomedical Engineering

ISSN: (Print) (Online) Journal homepage: https://www.tandfonline.com/loi/gcmb20

Numerical study of hemodynamics in a complete coronary bypass with venous and arterial grafts and different degrees of stenosis

Shila Alizadehghobadi , Hasan Biglari , Hanieh Niroomand-Oscuii & Meisam H. Matin

To cite this article: Shila Alizadehghobadi , Hasan Biglari , Hanieh Niroomand-Oscuii & Meisam H. Matin (2020): Numerical study of hemodynamics in a complete coronary bypass with venous and arterial grafts and different degrees of stenosis, Computer Methods in Biomechanics and Biomedical Engineering, DOI: 10.1080/10255842.2020.1857744

To link to this article: https://doi.org/10.1080/10255842.2020.1857744

Published online: 12 Dec 2020.

COMPUTER METHODS IN BIOMECHANICS AND BIOMEDICAL ENGINEERING
https://doi.org/10.1080/10255842.2020.1857744

Numerical study of hemodynamics in a complete coronary bypass with venous and arterial grafts and different degrees of stenosis

Shila Alizadehghobadi[a], Hasan Biglari[a], Hanieh Niroomand-Oscuii[b] and Meisam H. Matin[c]

[a]Department of Mechanical Engineering, University of Tabriz, Tabriz, Iran; [b]Department of Mechanical Engineering, Sahand University of Technology, Tabriz, Iran; [c]Department of Mechanical and Aerospace Engineering, University of Florida, Gainesville, FL, USA

ABSTRACT

Cardiovascular diseases are among the leading causes of death in the world. The coronary blockage is one of most common types of these diseases that in the majority of cases has been treated by bypass surgery. In the bypass surgery, a graft is implemented to alter the blocked coronary and allow the blood supply process. The hemodynamic characteristics of the bypass strongly depend on the geometry and mechanical properties of the graft. In the present study, the fluid-structure interaction (FSI) analysis is conducted to investigate the bypass performance for a thoracic artery as well as a saphenous vein graft. Blood flow introduces a pressure on the walls of the graft which behaves as a hyperelastic material. A complete coronary bypass with stenosis degrees of 70% and 100% is modeled. To consider the nonlinear stress-strain behavior of the grafts, a five parameter Mooney-Rivlin hyperplastic model is implemented for the structural analysis and blood is assumed to behave as a Newtonian fluid. The simulations are performed for a structured grid to solve the governing equations using finite element method (FEM). The results show that wall shear stress (WSS) for saphenous vein is larger than that of thoracic artery while the total deformation of the thoracic artery is larger compared to the saphenous vein. Also, for the venous grafts or lower stenosis degree, the oscillatory shear index (OSI) is higher at both left and right anastomoses meaning that venous grafts as well as lower degree of stenosis are more critical in terms of restenosis.

ARTICLE HISTORY
Received 9 April 2020
Accepted 26 November 2020

KEYWORDS
Coronary bypass; fluid-structure interaction (FSI); blood flow; hyperelastic model; stenosis

1. Introduction

One of the most prevalent cardiovascular diseases is coronary artery disease which is the leading cause of death all over the world (Wong 2014). The stenosis or blockage of the artery brings about a reduction of blood flow to the heart muscle and therefore causes problems for blood supply to the heart. One of the main treatments for the coronary artery blockage is bypass surgery in which an alternative graft is used to compensate for the blood flow reduction through the coronary artery (Arima et al. 2005; Deb et al. 2013). This graft is connected to the aorta from upstream and to the coronary artery from downstream. Internal thoracic artery (ITA) and small saphenous vein are the commonly used vessels in bypass. The main issue encountered after the bypass surgery is stenosis or partial blockage of the graft which occurs due to the variations in the hemodynamic conditions leading to the failure of the grafting. The hemodynamic conditions strongly depends on the mechanical properties of the artery tissues. Since the accurate experimental evaluation of the parameters is almost elusive due to the challenges associated with the ultrasonic velocity measurement, numerical simulations can examine the flow conditions and hemodynamics conveniently but with some limitations. Owida et al. (2012) provided an overview on numerical simulations of the flow pattern and wall shear stress in the occluded coronary arteries.

In a pioneering study, Hofer et al. (1996) numerically modeled the end-to-side anastomoses with an idealized geometry to examine the influence of compliance mismatch on wall mechanics and blood flow implementing two distensible models with different graft elasticity. They coupled Navier-Stokes equations for the flow with the nonlinear shell model for the vessel wall. They reported that although the normal deformation of the wall increases by the elasticity, the maximum displacement and areas of high shear stress are more prevalent in the junction region along the graft-artery intersection and not affected by the elasticity of the model.

CONTACT Hasan Biglari hbiglari@tabrizu.ac.ir; Meisam H. Matin mhabibi@ufl.edu

The numerical results of Vimmr et al. (2013) for patient specific aorta-coronary bypasses suggested that considering the Newtonian model for the blood properties does not cause significant discrepancy in the results of the blood flow. This is while the results of Chen et al. (2006) for idealized geometry of a coronary artery with 75% stenosis, and Guerciotti and Vergara (2018) for patient-specific stenotic coronary and carotid cases, revealed a discrepancy in the wall shear stress and flow characteristics for non-Newtonian versus Newtonian model. It was also reported by Guerciotti and Vergara (2018) that by increasing the stenosis severity, the discrepancy became more pronounced. Kamangar et al. (2017). conducted a computational analysis to investigate how the stenosis affects the hemodynamics of blood flow in coronary arteries. They found that higher wall shear stress associated with the stenosed coronary might result in the platelets activation and coronary artery failure. They also observed low wall shear stress downward the stenosis that caused a recirculation area that can form another stenosis after a while and then serial stenoses may form (Hoque et al. 2020). Guerciotti et al. (2017) observed that the low stenosis degree in the left anterior descending (LAD) coronary artery may cause a disturb flow at the anastomosis between LAD and left internal mammary artery (LIMA) which is associated with stagnation areas and may lead to restenosis. Similar results were observed by Zhang et al. (2008) and Ding et al. (2012) for complete coronary artery and LIMA-LAD bypass grafts, respectively, showing that decreasing the degree of stenosis results in a higher risk of atherogenesis and graft failure.

Chaichana et al. (2014) aimed at the assessment of the influence of plaque on the shear stress and pressure stress gradient on the wall of the left side coronary artery. They located plaques at the left main stem to generate a stenosis greater than 50%. Their results suggest that the presence of plaques results in a reduction in the wall shear stress while increases the wall pressure stress gradient. By using a fluid-structure interaction (FSI) simulation, Tang et al. (2003) investigated the influence of asymmetric stenosis of carotid arteries including stenosis severity, eccentricity, and pressure conditions on blood flow characteristics and stress distribution in the artery's wall. They deployed a hyperelastic model in their analysis in order to take into account the nonlinear elastic behavior of the artery's wall. They suggested that stenosis severity may lead to higher normal stress in the wall as well as higher shear stress in the stenosed region. Guerciotti et al. (2017) numerically investigated the possibility of graft failure if arterial or venous vessels are used in coronary bypass grafting. Their results demonstrated that the use of a vein for grafting leads to higher stresses on vessel wall compared to the arterial case. The effect of anastomosis configuration was investigated by Matsuura et al. (2018) and Koksungnoen et al. (2018) and it was suggested that the anastomosis angle of 45° results in lower shear stress on the walls which makes this configuration the most effective case in prevention of the bypass failure. As of late, a patient-specific 3 D simulation that implemented FSI method disclosed that using the venous and arterial grafts lead to different mechanical stimuli in coronary bypass surgery (Ramachandra et al. 2016). This study was conducted for the cases with no graft stenosis.

In the previous studies, the effect of the type of graft is not investigated on the complete coronary bypass taking into account the interaction of the blood and vessel, the hyperelastic behavior of the grafts and the graft stenosis. In the present work, we study two different grafts as thoracic artery and saphenous vein for a complete coronary bypass with both proximal and distal parts and then compare the hemodynamics of them for 100% and 70% stenotic cases. The simulation is based on FSI modeling and hence flow problem is coupled with the structural problem to find the blood velocity, stress distributions throughout the wall and deformation of the wall. For this purpose the Navier-Stokes equations along with the stress equations are solved in a time-dependent form. A five parameter Mooney-Rivlin hyperplastic model is implemented for the structural analysis and blood is assumed to behave as a Newtonian fluid.

2. Materials and methods

A three dimensional coronary bypass model is considered to investigate the effect of the graft material on the hemodynamics of the coronary bypass. Two different grafts are considered with the properties of saphenous vein and thoracic artery. The schematic of the geometry along with the dimensions are represented in Figure 1. The artery and vein are modeled as a single layer tissue and the geometry is generated using SOLIDWORKS software. Since the flow in each part of the arteries is axisymmetric, one half of the geometry is drawn in order to be more efficient in terms of CPU time and data saving. Solving this problem requires a coupled fluid-structural analysis of the blood-vessel system that takes into consideration

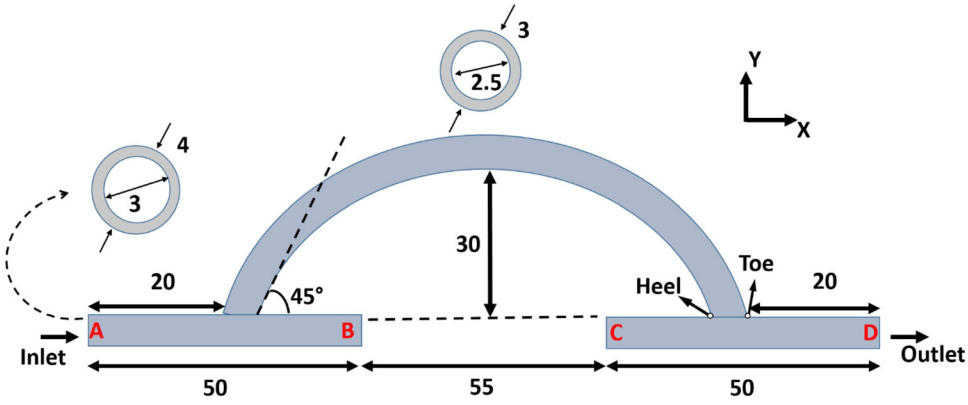

Figure 1. 2 D schematic of the geometry and dimensions.

the interfacial interaction between the thoracic artery (or saphenous vein) wall and the blood. The blood is assumed to behave like a Newtonian fluid with constant properties and be at the same temperature as the vessel and hence the flow is isothermal. Since the Reynolds number is in the laminar range (Re $<$ 2300) the incompressible Navier-Stokes equations are governing the blood flow:

$$\vec{\nabla}.\vec{V} = 0 \tag{1}$$

$$\frac{\partial \vec{V}}{\partial t} + \vec{V}.\vec{\nabla}\vec{V} + \frac{\vec{\nabla}P}{\rho} - 2\frac{\eta}{\rho}\vec{\nabla}.D = \vec{0} \tag{2}$$

where $\vec{V}$ and P stand for the velocity and pressure fields in the blood, respectively, and D represents the tensor operator. μ and ρ are the dynamic viscosity and density of blood, respectively. The equation governing the structural equilibrium can be written in the form of:

$$\frac{\partial}{\partial x^l}\left[T^{jl}\left(\frac{\partial u^k}{\partial x^j} + \delta_j^k\right) + \rho_0 f_0^k\right] = 0 \tag{3}$$

in which u is the velocity component and T^{jl} is the Piola-Kirchhoff stress tensor and δ_j is the deformation. f_0 and ρ_0 are the vector of initial forces applied on the system and density, respectively. The governing equations (Eqs. (1)-(3)) are subject to the following boundary conditions at the fluid-structure interface:

$$\vec{V} = 0 \tag{4-a}$$

$$\delta_f = \delta_s \tag{4-b}$$

$$\sigma_f^{ji}.\vec{n} - \sigma_s^{ji}.\vec{n} = 0 \tag{4-c}$$

where σ_f and σ_s are the stress tensor for the fluid and the Cauchy stress tensor for the vessel wall, respectively, and $\vec{n}$ is the normal vector. Eq. (4-a) represents the no-slip condition as well as the impermeability of the wall and Eqs. (4-b) and (4-c) stand for the continuity of the displacement and traction at the interface, respectively.

Since the linear elastic model is unable to predict the nonlinear stress-strain behavior of the arterial wall, the wall is assumed to exhibit a hyperelastic behavior and for this purpose, the nonlinear Mooney-Rivlin model is implemented in the material section of the software. Several investigations have confirmed the validity of this model for prediction of cardiac tissue's structural behavior (Holzapfel et al. 1996; Holzapfel and Gasser 2001; Khanafer et al. 2009). The following function represents the strain energy density for the Mooney–Rivlin model:

$$\begin{aligned} W = {} & C_{10}(I_1 - 3) + C_{01}(I_2 - 3) + C_{20}(I_1 - 3)^2 \\ & + C_{11}(I_1 - 3)(I_2 - 3) + \\ & C_{02}(I_2 - 3)^2 + \frac{1}{D}\left(J^2 - 1\right) \end{aligned} \tag{5}$$

in which W is a function of two main invariants I_1 and I_2 :

$$\begin{aligned} W &= W(I_1, I_2), I_1 = \lambda_1^2 + \lambda_2^2 + \lambda_3^2, I_2 \\ &= \lambda_1^2\lambda_2^2 + \lambda_1^2\lambda_3^2 + \lambda_2^2\lambda_3^2 \end{aligned} \tag{6}$$

where λ_1^2, λ_2^2, λ_3^2 are the squares of stretch ratios and are assumed to be incompressible

$$\lambda_1 * \lambda_2 * \lambda_3 = 1, \tag{7}$$

Det J = 1

Owing to an incompressibility assumption (Karimi et al. 2014), J is equal to unity and hence the last term in Mooney-Rivlin formulation (Eq. (5)) vanishes. The Mooney-Rivlin coefficients C_{10} ،C_{01} ،C_{20} C_{11} ، C_{02} are obtained from the results of tensile tests performed for each arterial material (Karimi et al. 2014; Razaghi et al. 2016; Karimi et al. 2017) and provided in Table 1. Introducing a relative coordinate system, Navier-Stokes equations in Arbitrary Lagrangian-Eulerian (ALE) form can be written as:

Table 1. Mooney-Rivlin coefficients (Karimi et al. 2014; Razaghi et al. 2016; Karimi et al. 2017).

	C_{10} (MPa)	C_{01} (MPa)	C_{02} (MPa)	C_{20} (MPa)	C_{11} (MPa)
Saphenous vein	9.392	−8.828	0.014	−5.627	5.523
Thoracic artery	0.115	−0.049	2.201	1.403	−3.370

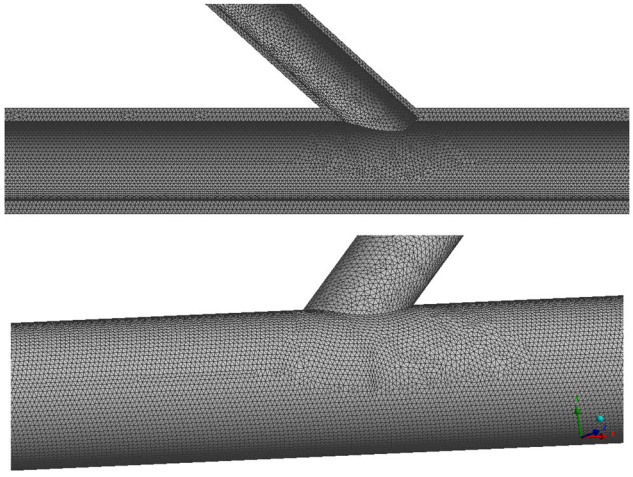

Figure 2. Inside view (top) and outside view (bottom) of the generated grid.

$$\frac{\&u_j}{\&x_j} = 0, \quad j = 1, 2, 3 \tag{8}$$

$$\rho\left(\frac{\delta u_i}{\delta t} + (u_j - \widehat{u_j})\frac{\delta u_i}{\delta x_j}\right) - \frac{\delta}{\delta x_j}\left(\mu\left(\frac{\delta u_i}{\delta x_j} - \frac{\delta u_j}{\delta x_i}\right)\right) + \frac{\delta P}{\delta x_i} = 0 \tag{9}$$

with u_j (j = 1,2 and 3) being the components of the flow velocity and $\widehat{u_j}$ (j = 1,2 and 3) being the components of domain velocity, respectively.

3. Numerical solution

To have a more stable solution an unstructured grid with triangular elements is generated. The element size is 0.1 mm and the total number of the nodes and elements are 4349541 and 2226299, respectively. Two views of the generated grid are shown in Figure 2. The transient FSI is simulated using ANSYS Workbench V16.0 (ANSYS, Inc.). It implicitly couples a fluid solver (ANSYS Fluent) to solve the blood flow with a structural solver (ANSYS Mechanical) to solve the vascular wall deformation (ANSYS Inc 2016). The ALE formulation was utilized to solve the fluid domain features. The fluid solver resolves the Navier-Stokes equations along with the mass continuity based on the control volume. The laminar model is assumed in the solver and the second order upwind scheme is used for discretization

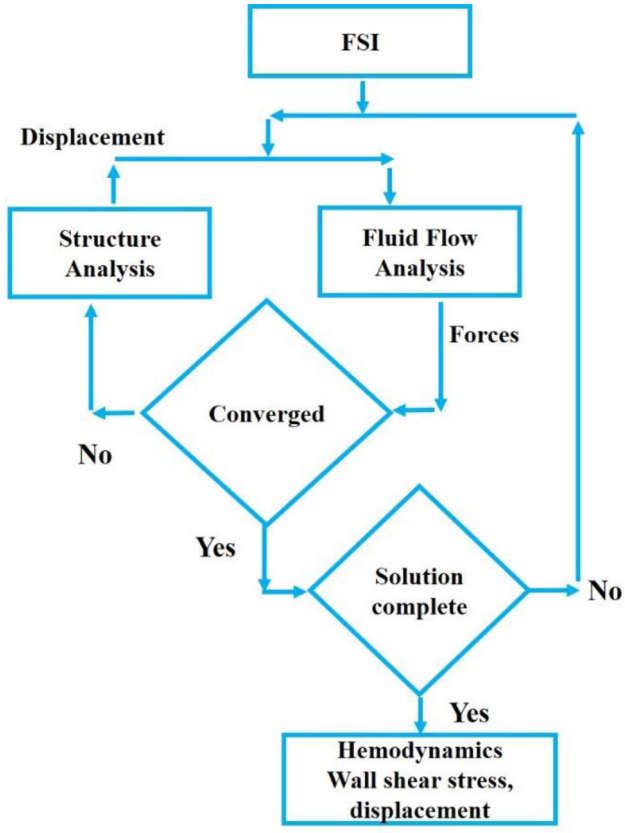

Figure 3. Flow chart of the system coupling and solution process.

of the fluid domain governing equations. The structural solver, based on an FEM, uses a Lagrangian multiplier-based mixed u-P formulation.

The two-way implicit coupling is used in the staggered strong coupling algorithm to accurately couple the fluid field and solid displacements. Although the solution of two-way coupling is slower than the one-way coupling, it is more accurate especially when the solid deformations (displacements) are as large as they affect the flow characteristics. In the two-way coupling the flow field and solid displacement are solved simultaneously and they correct each other at any time step. For instance, the pressure field in fluid solver (Fluent) is solved first and then it is transferred to the structural solver to yield the displacements and then it is again transferred to the fluid solver to upgrade the pressure field and this continues to reach an acceptable error in the solutions. The flowchart of the solution procedure and system coupling is presented in Figure 3. The details can be found in (Galpin et al. 1995).

4. Boundary conditions

The deformation of the arterial solid wall in all directions at the inlet and outlet is set to zero (sections A

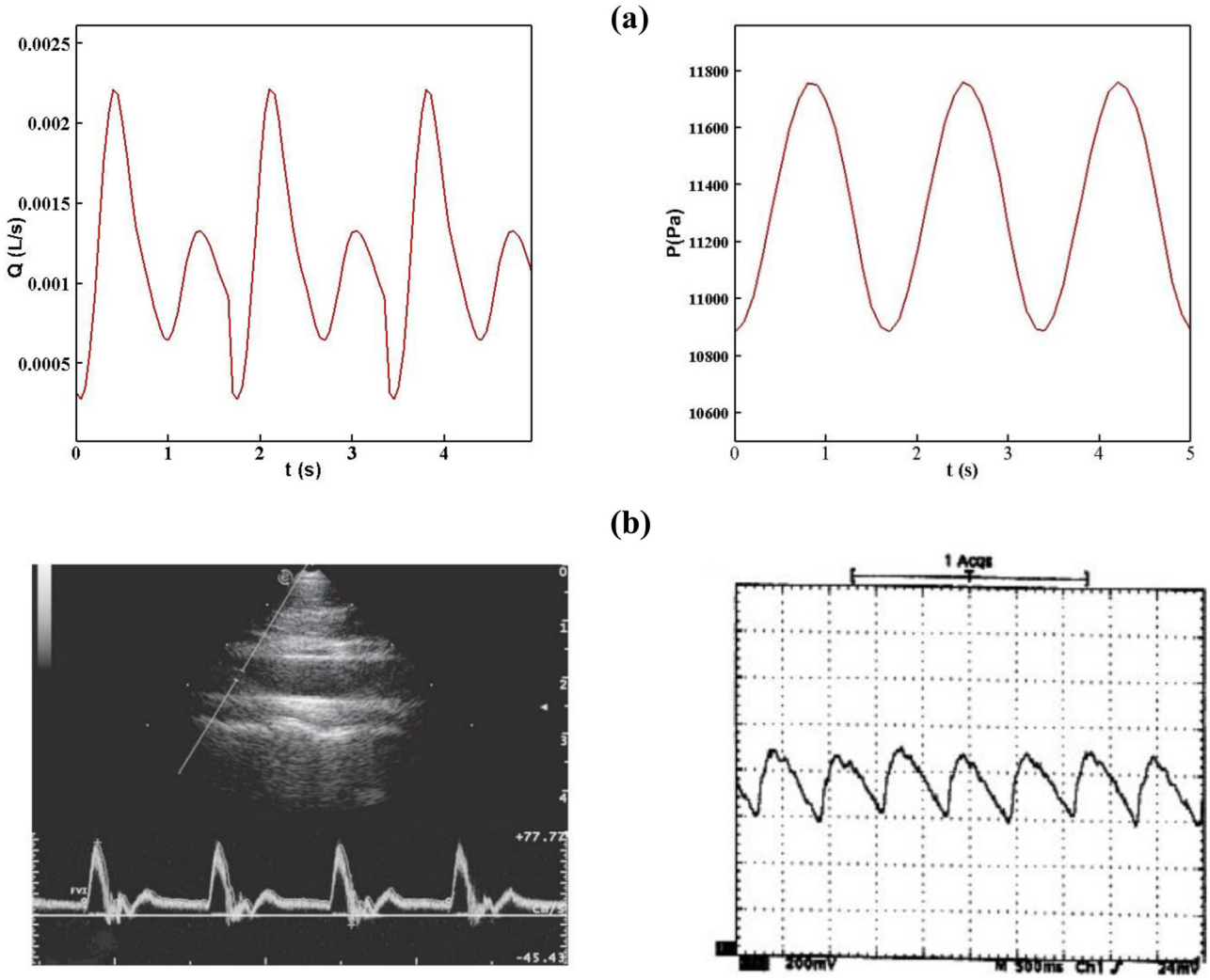

Figure 4. Volume flow rate and pressure pulsatile (a) Fourier series form and (b) actual pulses (Nichols and O Rourke 1998; Kawahito et al. 2000; Bertolotti et al. 2001; Kawahito et al. 2001; Vimmr et al. 2013).

and D in Figure 1) implying that the inlet and outlet are fixed. In the blockage cross sections (sections B and C in Figure 1), the solid can freely move in axial direction (x) and is fixed in radial directions (y and z). No constraint is imposed on the outer surface of the arterial wall to allow it to freely move in all directions. In some of the previous studies the Robin boundary condition was imposed (Moireau et al. 2012; Nobile et al. 2013) on the outer wall of the vessel to take into account the viscoelastic behavior of the tissues surrounding the artery. This Robin boundary condition physically means a support at the outer surface and considers the tissue an elastic body. Time-dependent mass flow rate and pressure are considered as the inlet and outlet boundary conditions. These inlet and outlet boundary conditions (shown in Figure 4) are based on a physiological pulsatile flow rate and pressure at the aorta (Nichols and O Rourke 1998; Kawahito et al. 2000; Bertolotti et al. 2001; Kawahito et al. 2001) reconstructed using a Fourier series. The Fourier series were input into ANSYS Fluent as a UDF file to define boundary conditions. The pulsatile form of the inlet flow rate and the outlet pressure, respectively, are as follows (Donovan et al. 1990):

$$Q(t) = \overline{Q} + \sum_{j=1}^{5} Q_j \cos\ (jwt - \phi_j) \tag{10}$$

$$P_{out}(t) = \overline{P} + \sum_{j=1}^{4} a_j^p\ \cos(jwt) + b_j^p\ \sin(jwt) \tag{11}$$

$\overline{Q}$ is the mean volume flow rate which is equal to 0.00108 L/s and w is the angular frequency with the time period of T = 1.68s. $\overline{P}$ is the mean pressure equal to 11328.67 *pa*. The above pulsatile conditions resemble the actual conditions for a healthy individual. All the coefficients are presented in Table 2.

Table 2. Coefficients of Fourier series for volumetric flow rate and pressure pulsatile [6,30].

J	b_j^p	a_j^p	ϕ_j[rad]	Q_j [L/s]
1	−2.2932	−3.3170	1.944	0.00030
2	8.0487	−9.8639	2.836	0.00058
3	3.8009	−3.0278	−2.124	0.00020
4	−3.2564	2.2476	−1.875	0.00015
5	–	–	−0.447	0.00005

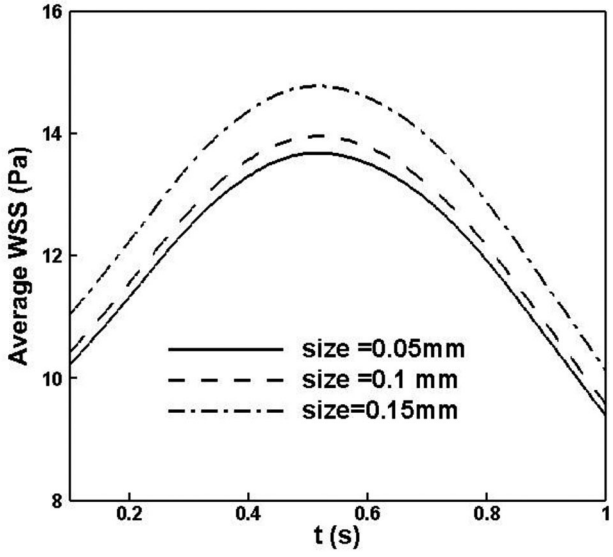

Figure 5. Grid dependence check.

5. Results and discussion

The triangular elements are used for the grid to have a more stable numerical solution. The time step and the number of iterations were 0.01 s and 50, respectively, to reach the convergence (with the residual of 0.0001 for velocities, pressure and stresses) and 0.8 was selected as the relaxation factor in the FSI coupling. Since the numerical solutions might be dependent on the size of the elements, the results of wall shear stress (WSS) on the thoracic artery wall for three different grid sizes are compared in Figure 5 to assure that the solution is independent of the element size. As is evident, decreasing the mesh size increasingly decreases the discrepancy between the results obtained for different sizes. Although the element size of 0.05 mm is the most accurate, it hugely increases the CPU time and since in the worst case scenario there is 2% error between the results for the element sizes of 0.05 and 0.1, therefore, the element size of 0.1 seems to be the most efficient grid for this problem.

To check the validity of the solution, the values of WSS obtained from the present study are compared with the results reported by Dong et al. (2015) for left coronary artery illustrated in Figure 6 alongside their

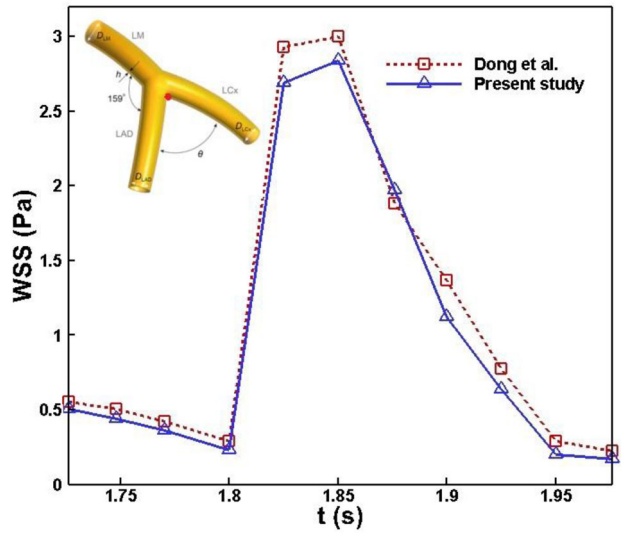

Figure 6. Comparison between the present solution with the results of Dong et al. (Dong et al. 2015).

geometry. The point for which we did the validation is marked in red and the results are presented for angulation of 90°. It is obvious that there is a good agreement between the present solution and the results of Dong et al. (2015).

Figure 7 represents the velocity contours versus time for different cross sections in the coronary for both thoracic artery and saphenous vein. Regardless of the coronary material at the graft exit, the velocity contour has an eccentricity toward the wall. This is because the acceleration of the blood is positive in x direction when it is falling from the peak (cross section B-B) and this acceleration pushes the blood toward the wall. This eccentricity is more pronounced for saphenous vein. The contours at the graft entry are almost the same for both thoracic artery and saphenous vein. As it is expected the velocity profile for t = 0.5s is maximum because the flow rate at the inlet gets its maximum value at this time. The velocity contours along both the occluded and 70% stenosis coronary are depicted in Figure 8 for thoracic artery and saphenous vein. As it can be seen, independent of the graft type, the flow pattern for both is the same. For the occluded case, in the thoracic artery the velocity at the graft entry is almost uniform and gradually develops to reach its maximum at the highest height of the graft and thereafter it decreases to the point that the blood leaves the graft as a fluid jet. Diminishing the velocity when the blood is falling down to the exit point is due to the absorption of kinetic energy of the blood by the coronary wall throughout the graft. However for the saphenous vein the story is completely different and the velocity distribution is almost the same at all the cross sections

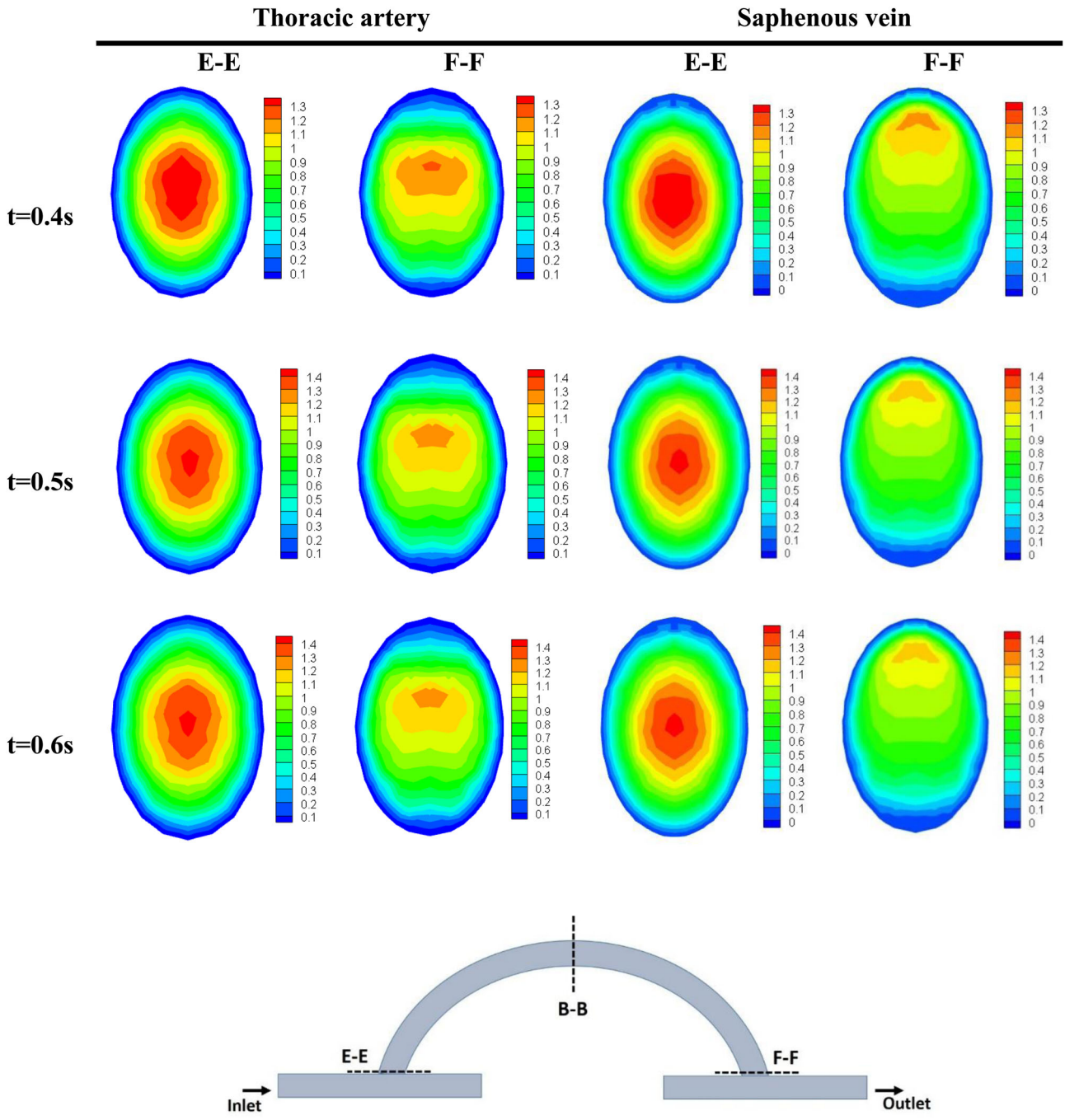

Figure 7. Velocity contours for different cross sections and different times for both thoracic artery (left) and saphenous vein (right).

throughout the graft. This is because the saphenous vein is more elastic than the thoracic artery and it does not absorb the kinetic energy of the blood by its deformation. For the case of 70% stenosis, regardless of the graft type, a larger portion of the flow goes through the stenosed coronary rather than the graft causing the higher velocity gradients at the partially occluded zone. A quick glance at Figure 8 tells us that at the same conditions, the blood flow in the saphenous vein is always faster (higher velocity) than the thoracic artery. It should be noted that at the left side of the exit blood flow, there is a rotational back flow which is cause of the relatively oscillating shear at this region and makes this region more potent to the restenosis. The rotational flow regions increases the time of residence of the blood on the walls increases and the blood cells find more time to transfer mass to the walls. The contours also depict that at

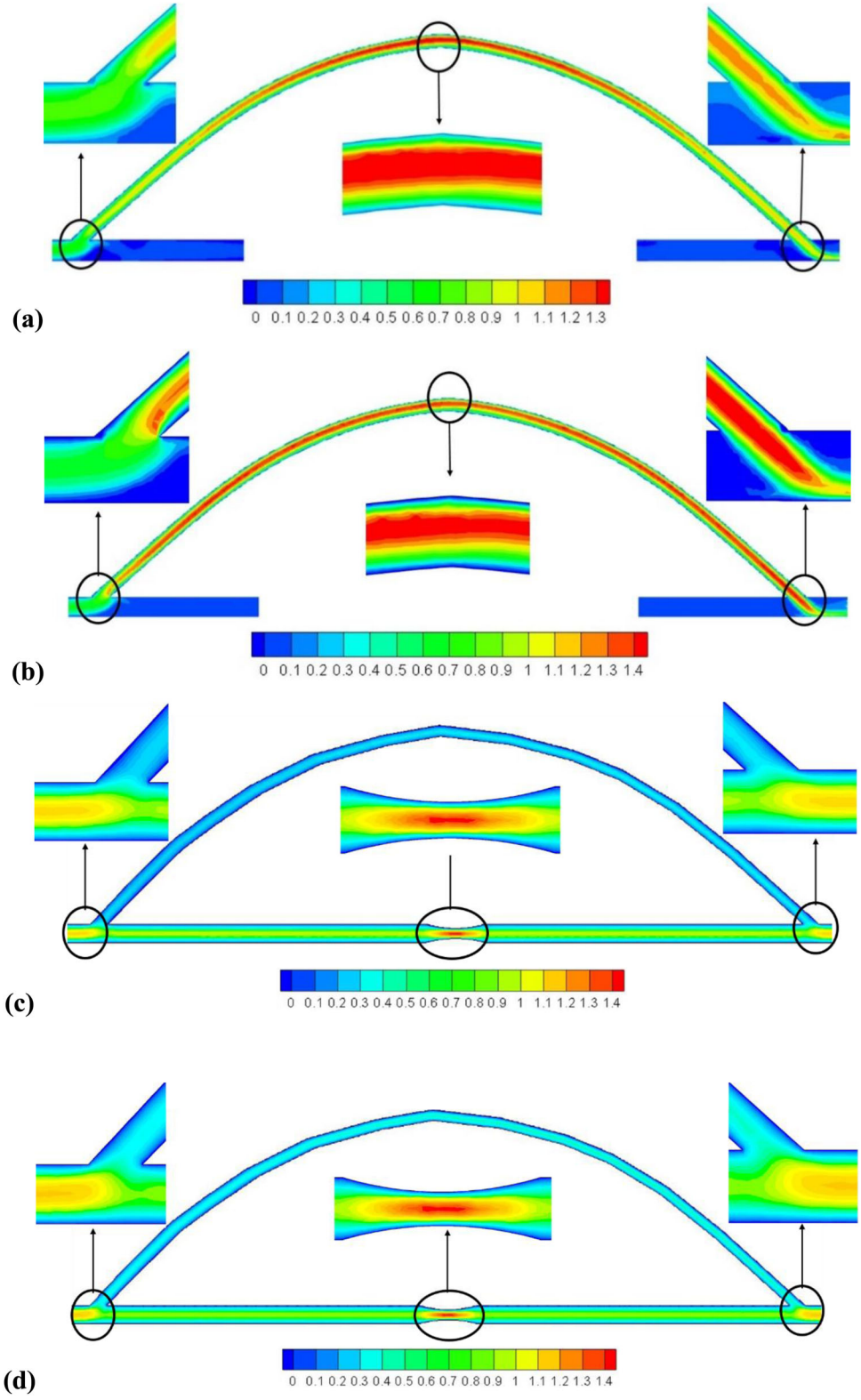

Figure 8. Velocity contours (m/s) for (a) occluded case with arterial graft, (b) occluded case with venous graft, (c) 70% stenosis with arterial graft, and (d) 70% stenosis with venous graft.

the blood circulation in the occluded regions is very weak and this might increase the sedimentation process at these regions.

Table 3 presents the radial deformation (mm) of the thoracic artery and saphenous vein against time at different cross sections. As it is obvious, the radial

Table 3. Radial deformation (mm) for thoracic artery and saphenous vein for different cross sections.

	E-E		B-B		F-F	
time	Thoracic artery	Saphenous vein	Thoracic artery	Saphenous vein	Thoracic artery	Saphenous vein
0.1	0.02139	0.005863	0.010449	0.002936	0.007798	0.002064
0.2	0.021374	0.005761	0.014161	0.003918	0.001968	0.000521
0.3	0.023461	0.006342	0.017118	0.004570	0.002003	0.000522
0.4	0.025004	0.006753	0.019031	0.005044	0.00197	0.000531
0.5	0.02559	0.006941	0.01877	0.005228	0.001831	0.000526
0.6	0.025235	0.006792	0.018815	0.005136	0.001292	0.000335
0.7	0.024089	0.006480	0.018296	0.004799	0.001077	0.000278
0.8	0.02227	0.005972	0.015747	0.004173	0.000746	0.000168
0.9	0.019916	0.005341	0.01301	0.003442	0.000571	0.000129
1	0.01752	0.004691	0.010586	0.002786	0.000335	0.0000878

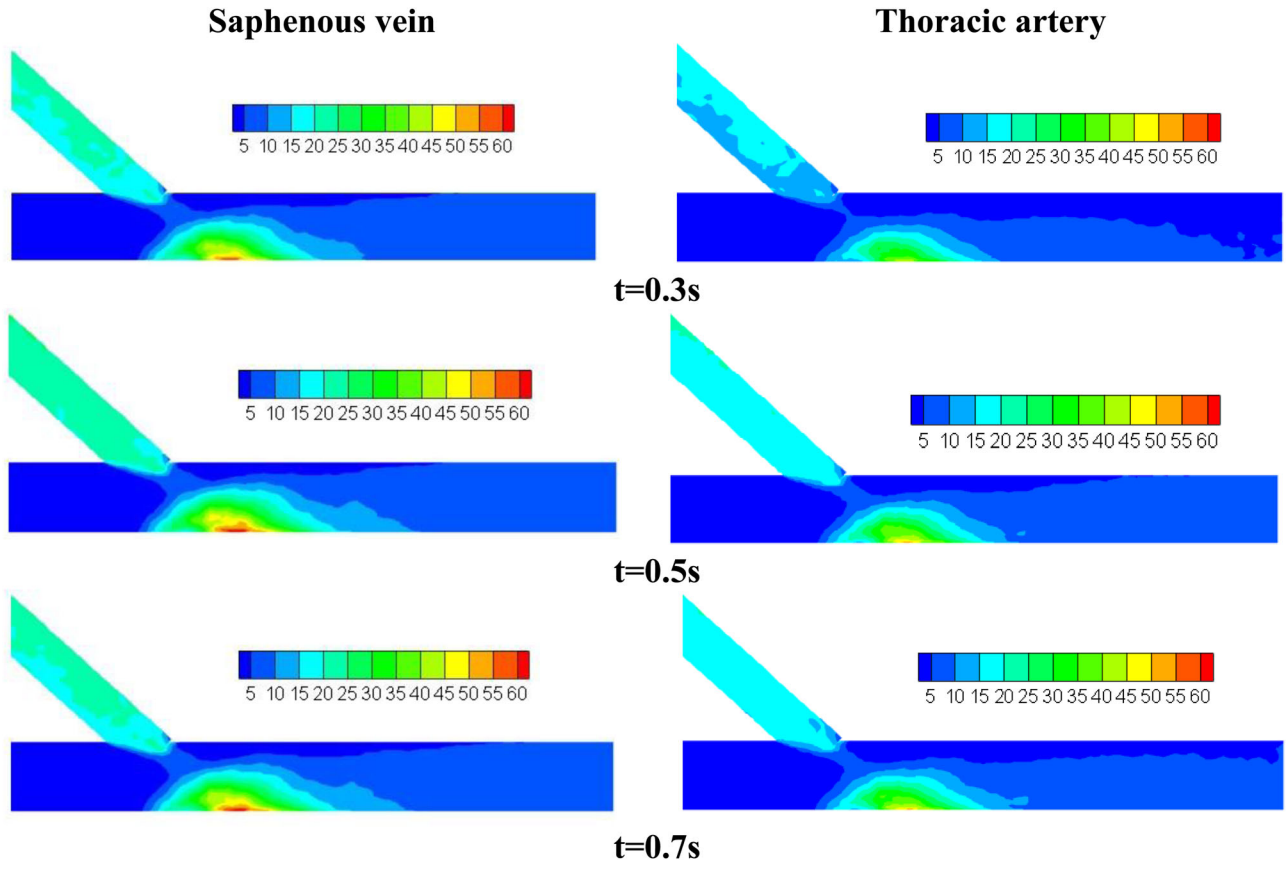

Figure 9. Wall shear stress (Pa) at the right side coronary at different times.

deformation of the thoracic artery is substantially larger than that of saphenous vein at any cross section and any time. At any time the radial deformation for the cross section E-E (graft inlet) is maximum and at cross section F-F (graft exit) is minimum. The cross section B-B takes the values between these two. It is justifiable since at the inlet blood invades into the graft and it produces highest radial stress and consequently largest radial deformation. At F-F since the blood leaves the graft into a larger size tube it is reasonable to have a less deformation compared with the cross section B-B.

Figures 9 and 10 show the WSS contours for vein and artery for the right and left sides of the coronary at different times. As it is clear the WSS pattern for both is similar but the values are greater for vein. At $t = 0.5s$ that the inlet pulse is maximum the WSS is larger than other times since at with the increase in inlet velocity the velocity gradient on the wall and consequently shear stress increase. It is worth mentioning that the shear stress at the bottom wall on the right side coronary and next to the exit is substantially larger than other regions in the bypass coronary. This is because the blood is sprayed on the wall next

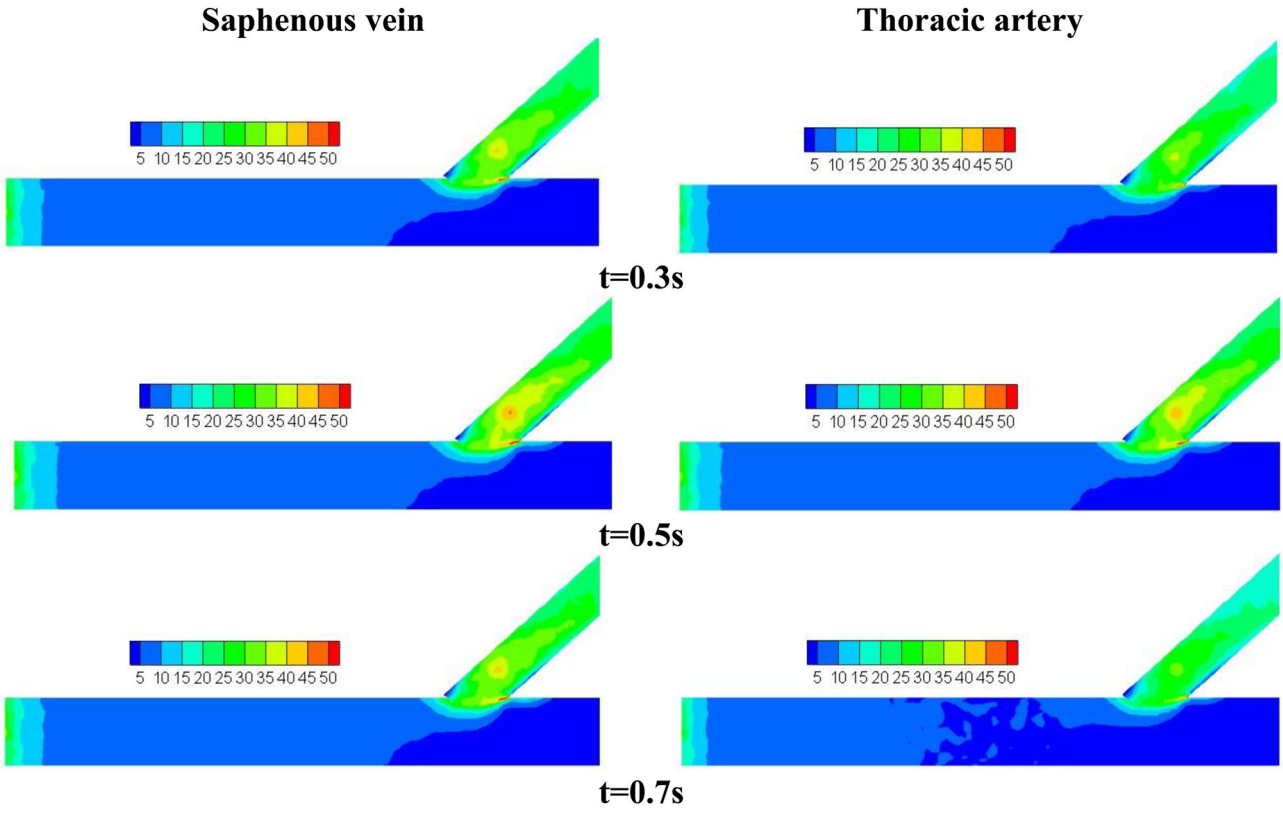

Figure 10. Wall shear stress (Pa) at the left side coronary at different times.

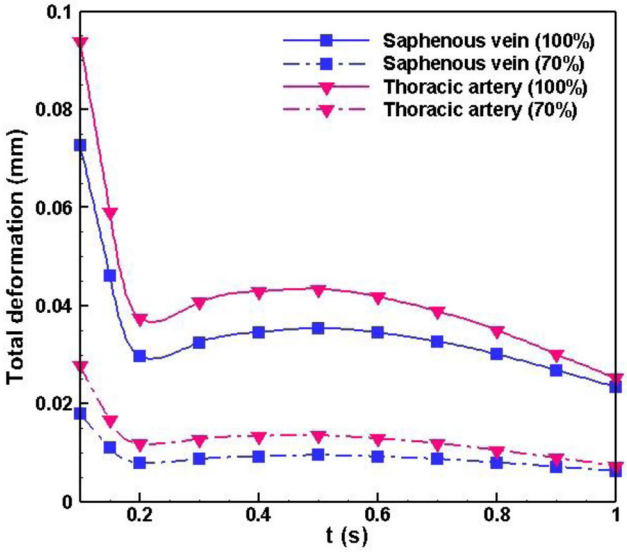

Figure 11. Total deformation for saphenous vein and thoracic artery as function of time.

to the exit and has to change its direction slipping on the wall and this produces relatively large shear stresses up to 5 times larger than other areas on the coronary wall. It can be observed that at the outlet of the coronary bypass the shear stress becomes uniform since the flow is fully developed. Furthermore, the WSS in the graft is up to 5 times that in the main vessel except for the wall next to the graft exit. Physically speaking, since the graft has a smaller diameter than the main vessel, its flow is associated with larger pressure drop and then larger friction (shear stress).

The results also show that regions with low WSS in the thoracic artery are more distributed than saphenous vein. It implies that the sedimentation and blockage are more probable in the thoracic artery than saphenous vein after bypass surgery. It should be noted that the regions with low WSS are more susceptible to sedimentation and blockage and these regions in the saphenous vein are a little less present than the thoracic artery.

The total deformation of the coronary artery with saphenous vein graft as well as with thoracic artery graft is plotted in Figure 11 as a function of time. As it was mentioned earlier, the deformation in the thoracic artery is larger than the saphenous vein. This can be attributed to the higher stiffness of the saphenous vein that leads to its resistance against deformation while the thoracic artery is less stiff and experience a larger deformation. The maximum deformation happens at the beginning of the pulse because the blood is abruptly pumped through the coronary and make large deformations and after that while the pulse velocity is increasing the deformation first falls and then

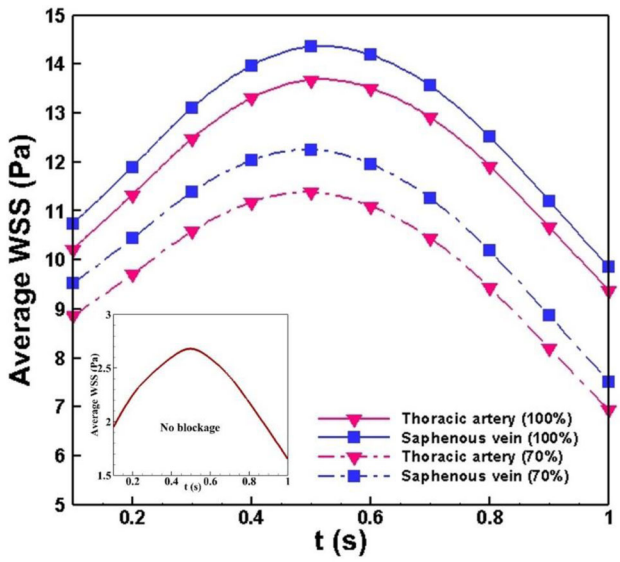

Figure 12. Average WSS for saphenous vein and thoracic artery as function of time.

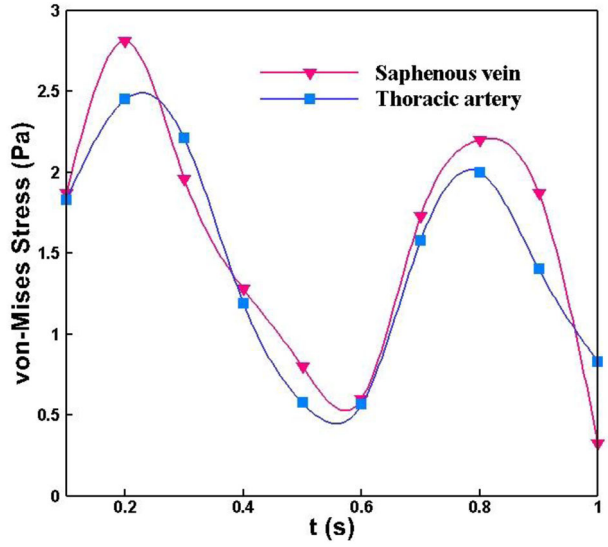

Figure 13. von-Mises stress for saphenous vein and thoracic artery grafts.

start increasing to reach a peak at t = 0.5s. The reason for the diminish of the deformation in the times before 0.2 s is that flow is becoming fully developed and a portion of its kinetic energy is spending for developing the flow but after t = 0.2s the entire energy is spent for wall deformation.

Figure 12 represents the average WSS versus time for the coronary with saphenous vein and thoracic artery grafts. The results for a healthy (no blockage) vessel is also shown for comparison. It can be seen that the WSS for the coronary with saphenous vein graft is always greater than that of thoracic artery graft meaning that more friction is experienced on the coronary wall when the vein is used and hence the heart needs higher pumping power in the case of vein graft. The comparison of these results with that of healthy vessel suggests that the WSS for the healthy vessel is much less than the grafted coronary. This is reasonable since the length of the graft produces an additional amount of pressure drop and then shear stress. Small diameter of the graft definitely contributes to this increment in the WSS for the coronary bypass compared with the healthy vessel.

The importance of von-Mises criterion is pronounced in the systems where there is a combination of normal and shear stresses that is clearly the case with this fluid-structure system. Therefore, examining the von-Mises criterion is to be considered in the design of the coronary artery systems. Figure 13 compares the von-Mises stresses in the internal wall of the saphenous and thoracic artery grafts. It seems that the temporal average of the stresses (area under the curve) for the saphenous graft is larger and also the maximum von-Mises stress for the saphenous graft is almost 12% greater. This is to say that under the same conditions, the saphenous graft reaches the yield stress before the thoracic artery graft and that is more critical from the viewpoint of design.

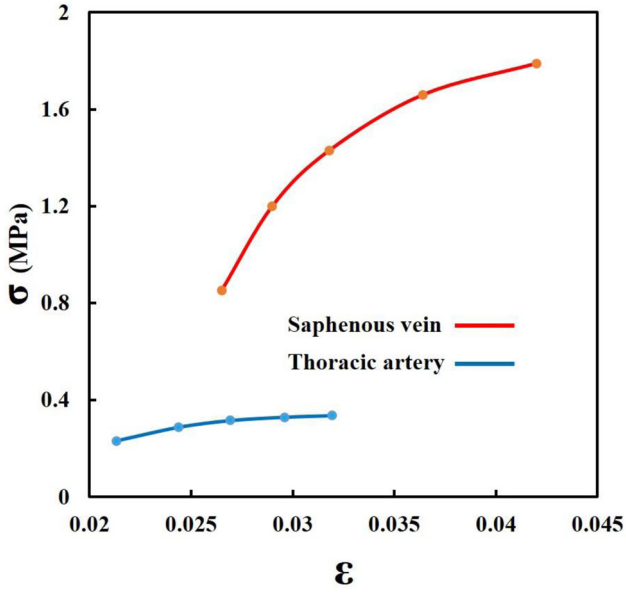

Figure 14. Stress-strain diagram for thoracic artery and saphenous grafts.

Based on Mooney-Rivlin model and regarding the results obtained for principal stress and strain for some points in the artery wall, the stress-strain graph is represented in Figure 14 for both saphenous and thoracic grafts. Clearly, the slope of the stress-strain graph for the saphenous graft is sharper compared to

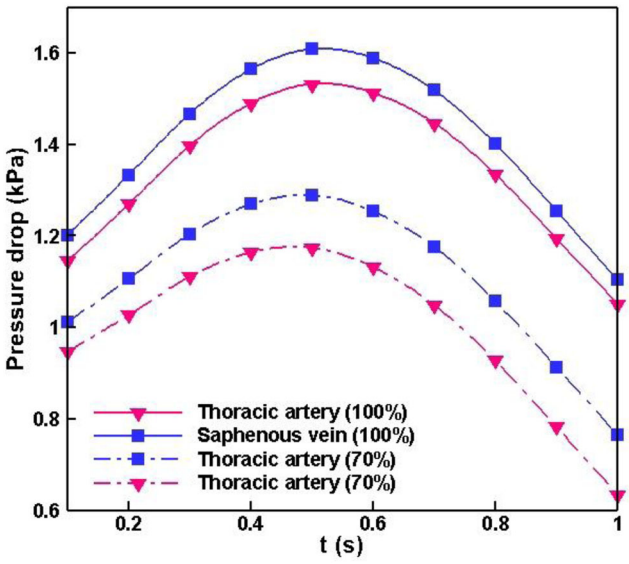

Figure 15. Blood pressure drop throughout the graft.

the thoracic, meaning that at the same flow conditions the stiffness (elasticity) of the saphenous graft is higher. It is also obvious that the strain energy density, $\sigma\varepsilon/2$, for the thoracic artery is larger than the saphenous graft.

Figure 15 indicates the blood pressure drop from the graft inlet to its outlet as function of time for saphenous and thoracic artery grafts. As is expected the pressure drop in the thoracic artery is more than saphenous graft. This difference is maximum at t = 0.5s that shows 7% difference. The pressure drop has a same trend as the wall shear stress since the pressure drop and wall shear stress are proportional for Newtonian fluids in a tube.

Oscillatory shear index is another quantity of interest that measures the temporal variations of local WSS and is defined as follow:

$$OSI = \frac{1}{2}\left(1 - \frac{\left|\int_0^T \tau_w \, dt\right|}{\int_0^T |\tau_w| \, dt}\right) \tag{12}$$

OSI can vary between 0 and 0.5. In the regions with high separation or stagnation zones where the reverse flow might happen, the values of OSI are higher. Oscillatory shear index is a criterion for the oscillating portion of the flow. Regions of disturbed and recirculating flow, which have high OSI, are known to be more potent to trigger intimal hyperplasia in the vessel wall, which consequently provides conditions conducive to restenosis. The results of OSI for toe and heel regions of the left and right anastomosis for arterial and venous grafts with two stenosis degrees (70% and 100%) are summarized in Table 4. It is obvious that for the venous grafts or lower

Table 4. Comparison of segmental average of oscillatory shear index for arterial and venous grafts and different degrees of stenosis.

	Artery (100%)	Vein (100%)	Artery (70%)	Vein (70%)
Right coronary heel	0.094	0.078	0.142	0.154
Right coronary toe	0.052	0.048	0.085	0.09
Left coronary heel	0.041	0.038	0.067	0.105
Left coronary toe	0.034	0.027	0.051	0.072

stenosis degree, the OSI is higher at both left and right anastomoses meaning that venous grafts as well as lower degree of stenosis are more critical in terms of restenosis. Also, regardless of the stenosis degree, the left anastomosis is less critical than the right one. Physically speaking, the lower degree of stenosis is associated with a competitive flow in the coronary that bring about a recirculation and an oscillating flow (Guerciotti et al., 2017). Average values of OSI obtained for the right coronary in our study (Table 4) confirm the results of Ding et al. (2012) for the right coronary (distal) that the increase in the stenosis degree would lead to a decrease in the OSI and lowering the probability of intimal hyperplasia and atherogenesis. Also our results show that for the right coronary (distal) heel the OSI is higher than the right coronary toe which confirm the results of Zhang et al. (2008) for the distal part of an arterial graft.

6. Limitations

There were some limitations in the numerical methodology implemented in this study. First, the geometry of coronary artery was considered to be idealized and was not constructed from the patient-specific medical images. The intention of using the idealized geometry is to provide a comparative investigation between different grafts and different stenosis degrees. This brings approximation to the results compared to the patient specific geometry. Second, vessel walls were assumed to be able to freely expand and not restricted on the outer surface. This resembles operating at the laboratory condition meaning that the viscoelastic behavior of the tissues surrounding the vessel was not taken into account. Third, process of arterialization in the saphenous vein which starts happening due to absorption of oxygen in lung after the bypass surgery and the possible molecular effect of the arterial grafts on the restenosis were not possible to be simulated using the FSI method which has a macroscopic nature. Therefore, the results of CFD simulations should be analyzed in-vivo. It should be mentioned that although the analysis of the time-dependent variation of the physical parameters in a

pulse is not the main objective of this study, it provides an insight into the phenomena that may increase the chance of restenosis.

7. Conclusion

The hemodynamic characteristics of the bypass strongly depend on the mechanical properties of the graft. In the present study, FSI analysis is conducted to investigate the bypass performance for artery and saphenous grafts. The FEM is considered and based on the numerical simulation the following concluding remarks can be made:

- The use of thoracic artery graft in comparison with the saphenous graft is associated with the lower average WSS meaning that the pressure drop and pumping power in the case of artery graft is less than that of saphenous graft.
- The total deformation for the coronaries with saphenous vein graft is less than that with thoracic artery graft and this implies that saphenous grafts are more durable because the failure in these grafts happens later compared to the thoracic artery grafts.
- The WSS in the wall next to the graft exit is larger than other areas in the coronary bypass. The regions with low shear stress which are more susceptible to the sedimentation and blockage in the thoracic artery case are more prevailing than that in the coronary with the saphenous vein graft.
- Velocity profile of the blood at the graft exit reveals a back flow in these regions regardless of the saphenous vein or thoracic artery graft.
- For the venous grafts with 70% stenosis, the OSI is higher at both left and right anastomoses than the thoracic artery, however, for the occluded case, the thoracic artery is more critical meaning that it is associated with higher OSI at both left and right anastomoses. Also, regardless of the stenosis degree, the left anastomosis is less critical than the right one.

It will be interesting to conduct a comprehensive study on the patient specific geometry for different stenotic cases and considering the venous arterialization in order to find optimal clinical conditions for coronary bypass in the long term.

Disclosure statement

No potential conflict of interest was reported by the author(s).

References

ANSYS Inc. 2016. ANSYS Academic Research, Release 16.0, Help System, ANSYS Inc.

Arima M, Kanoh T, Suzuki T, Kuremoto K, Tanimoto K, Oigawa T, Matsuda S. 2005. Serial angiographic follow-up beyond 10 years after coronary artery bypass grafting. Circ J. 69(8):896–902.

Bertolotti C, Deplano V, Fuseri J, Dupouy P. 2001. Numerical and experimental models of post-operative realistic flows in stenosed coronary bypasses. J Biomech. 34(8):1049–1064.

Chaichana T, Sun Z, Jewkes J. 2014. Impact of plaques in the left coronary artery on wall shear stress and pressure gradient in coronary side branches. Comput Methods Biomech Biomed Engin. 17(2):108–118.

Chen J, Lu X-Y, Wang W. 2006. Non-Newtonian effects of blood flow on hemodynamics in distal vascular graft anastomoses. J Biomech. 39(11):1983–1995.

Deb S, Wijeysundera HC, Ko DT, Tsubota H, Hill S, Fremes SE. 2013. Coronary artery bypass graft surgery vs percutaneous interventions in coronary revascularization: a systematic review. JAMA. 310(19):2086–2095.

Ding J, Liu Y, Wang F, Bai F. 2012. Impact of competitive flow on hemodynamics in coronary surgery: numerical study of ITA-LAD model. Comput Math Methods Med. 2012:356187.

Dong J, Sun Z, Inthavong K, Tu J. 2015. Fluid-structure interaction analysis of the left coronary artery with variable angulation. Comput Methods Biomech Biomed Engin. 18(14):1500–1508.

Donovan D, Schmidt SP, Townshend SP, Njus GO, Sharp WV. 1990. Material and structural characterization of human saphenous vein. J Vasc Surg. 12(5):531–537.

Galpin PF, Broberg RB, Hutchinson BR. 1995. Three-dimensional Navier-Stokes predictions of steady-state rotor/stator interaction with pitch change. Third Annual Conference of the CFD, Society of Canada, Banff, Alberta. Canada: Advanced Scientific Computing ltd.

Guerciotti B, Vergara C. 2018. Computational comparison between Newtonian and non-Newtonian blood rheologies in stenotic vessels. In: P. Wriggers and T. Lenarz editors. Biomedical technology, lecture notes in applied and computational mechanics. Vol. 84, Switzerland: Springer; p. 169–183.

Guerciotti B, Vergara C, Ippolito S, Quarteroni A, Antona C, Scrofani R. 2017. Computational study of the risk of restenosis in coronary bypasses. Biomech Model Mechanobiol. 16(1):313–332.

Guerciotti B, Vergara C, Ippolito S, Quarteroni A, Antona C, Scrofani R. 2017. A computational fluid-structure interaction analysis of coronary Y-grafts. Med Eng Phys. 47(1):117–127.

Hofer M, Rappitsch G, Perktold K, Trubel W, Schima H. 1996. Numerical study of wall mechanics and fluid dynamics in end-to-side anastomoses and correlation to intimal hyperplasia. J Biomech. 29(10):1297–1308.

Holzapfel GA, Eberlein R, Wriggers P, Weizsäcker HW. 1996. Large strain analysis of soft biological membranes: Formulation and finite element analysis. Comput Meth Appl Mech Eng. 132(1-2):45–61.

Holzapfel G, Gasser T. 2001. A viscoelastic model for fiber-reinforced composites at finite strains: Continuum basis, computational aspects and applications. Comput Meth Appl Mech Eng. 190(34):4379–4403.

Hoque KE, Ferdowsa M, Sawall S, Tzirtzilakis EE. 2020. The effect of hemodynamic parameters in patient-based coronary artery models with serial stenoses: normal and hypertension cases. Comput. Methods Biomech Biomed Eng. 23(9):467–475.

Kamangar S, Anjum Badruddin I, Badarudin A, Nik-Ghazali N, Govindaraju K, Salman Ahmed NJ, Yunus Khan TM. 2017. Influence of stenosis on hemodynamic parameters in the realistic left coronary artery under hyperemic conditions. Comput Methods Biomech Biomed Engin. 20(4):365–372.

Karimi A, Navidbakhsh M, Razaghi R, Haghpanahi M. 2014. A computational fluid-structure interaction model for plaque vulnerability assessment in atherosclerotic human coronary arteries. J Appl Phys. 115(14):144702.

Karimi A, Navidbakhs M, Rahmati SM, Sera T, Kudo S. 2017. A combination of experimental and numerical methods to investigate the role of strain rate on the mechanical properties and collagen fiber orientations of the healthy and atherosclerotic human coronary arteries. Bioengineered. 8(2):154–170.

Kawahito S, Takano T, Nakata K, Maeda T, Nonaka K, Linneweber J, Schulte-Eistrup S, Sato T, Mikami M, Glueck J, et al. 2001. Analysis of the Arterial Blood Pressure Waveform Using Fast Fourier Transform Technique During Left Ventricular Nonpulsatile Assistance. In Vitro Study. Artif. Organs. 24(7):850–853.

Kawahito S, Takano T, Nakata K, Maeda T, Nonaka K, Linneweber J, Schulte-Eistrup S, Sato T, Mikami M, Glueck J, Nosé, et al. 2000. Analysis of the arterial blood pressure waveform during left ventricular nonpulsatile assistance in animal models. Artif Organs. 24(10): 816–820.

Khanafer K, Bull J, Berguer R. 2009. Fluid–structure interaction of turbulent pulsatile flow within a flexible wall axisymmetric aortic aneurysm model. Europ J Mech/B Fluids. 28(1):88–102.

Koksungnoen S, Rattanadecho P, Wongchadakul P. 2018. 3D numerical model of blood flow in the coronary artery bypass graft during no pulse and pulse situations: Effects of an anastomotic angle and characteristics of fluid. J Mech Sci Technol. 32(9):4545–4552.

Matsuura K, Jin WW, Liu H, Matsumiya G. 2018. Computational fluid dynamics study of the end-side and sequential coronary artery bypass anastomoses in a native coronary occlusion model. Interact Cardiovasc Thorac Surg. 26(4):583–589.

Moireau P, Xiao N, Astorino M, Figueroa CA, Chapelle D, Taylor CA, Gerbeau J-F. 2012. External tissue support and fluid-structure simulation in blood flows. Biomech Model Mechanobiol. 11(1-2):1–18.

Nichols WW, O Rourke M. 1998. McDonald's blood flow in arteries: Theoretical, experimental and clinical principles. 4th ed. London: Arnold E.

Nobile F, Pozzoli M, Vergara C. 2013. Time accurate partitioned algorithms for the solution of fluid–structure interaction problems in haemodynamics. Comput Fluids. 86:470–482.

Owida AA, Do H, Morsi YS. 2012. Numerical analysis of coronary artery bypass grafts: an overview. Comput Meth Prog Biomed. 108(2):689–705.

Ramachandra A, Kahn A, Marsden A-L. 2016. Patient-specific simulations reveal significant differences in mechanical stimuli in venous and arterial coronary grafts. J Cardiovasc Transl Res. 9(4):279–290.

Razaghi R, Karimi A, Rahmani S, Navidbakhsh M. 2016. A computational fluid-structure interaction model of the blood flow in the healthy and varicose saphenous vein. Vascular. 24(3):254–263.

Tang D, Yang C, Kobayashi S, Zheng J, Vito RP. 2003. Effect of stenosis asymmetry on blood flow and artery compression: A three-dimensional fluid-structure interaction model. Ann Biomed Eng. 31(10):1182–1193.

Vimmr J, Jonášová A, Bublík O. 2013. Numerical analysis of non-Newtonian blood flow and wall shear stress in realistic single, double and triple aorto-coronary bypasses. Int J Numer Method Biomed Eng. 29(10): 1057–1081.

Wong ND. 2014. Epidemiological studies of CHD and the evolution of preventive cardiology. Nat Rev Cardiol. 11(5):276–289.

Zhang JM, Chua LP, Ghista DN, Yu SCM, Tan YS. 2008. Numerical investigation and identification of susceptible sites of atherosclerotic lesion formation in a complete coronary artery bypass model. Med Biol Eng Comput. 46(7):689–699.